LAWRENCE
LIVERMORE
NATIONAL
LABORATORY

UCRL-CONF-203167

A Distributed Activation Energy Model of Thermodynamically Inhibited Nucleation and Growth Reactions and its Application to the Phase Transition of HMX

Alan K. Burnham, Randall K. Weese, and Brandon L. Weeks

July 20, 2004

Submitted to the 32nd Annual Conference of the North American Thermal Analysis Society, Williamsburg, VA, October 4-6, 2004

A Distributed Activation Energy Model of Thermodynamically Inhibited Nucleation and Growth Reactions and its Application to the β–δ Phase Transition of HMX

Alan K. Burnham,* Randall K. Weese, and Brandon L. Weeks
Lawrence Livermore National Laboratory
Livermore, CA 94551-0808
burnham1@llnl.gov

ABSTRACT

Detailed and global models are presented for thermodynamically inhibited nucleation-growth reactions and applied to the β–δ Phase Transition of HMX (nitramine octahydro-1,3,5,7-tetranitro-1,3,5,7-tetrazocine). The detailed model contains separate kinetic parameters for the nucleation process, including an activation energy distribution resulting from a distribution of defect energies, and for movement of the resulting reaction interface within a single particle. A thermodynamic inhibition term is added to both processes so that the rates go to zero at the transition temperature. The global model adds the thermodynamic inhibition term to the extended Prout-Tompkins nucleation-growth formalism for single particles or powders. Model parameters are calibrated from differential scanning calorimetry data. The activation energy for nucleation (333 kJ/mol) is substantially higher than that for growth (29.3 kJ/mol). Use of a small activation energy distribution (~400 J/mol) for the defects improves the fit to a powered sample for both the early and late stages of the transition. The effective overall activation energy for the global model (208.8 kJ/mol) is in between that of nucleation and growth. Comparison of the two models with experiment indicates the thermodynamic inhibition term is more important than the energy distribution feature for this transition. Based on the applicability of the Prout-Tompkins kinetics approach to a wide range of organic and inorganic materials, both models should have equally broad applicability for thermodynamically constrained reactions.

INTRODUCTION

Solid-state reactions are generally governed by nucleation-growth phenomena. Solid-state phase transitions are a special case of nucleation-growth reactions. The two main lines of kinetic models for this process are the Prout-Tompkins (1) and Avrami-Erofeev (2,3) approaches. While originally derived for solid-state reactions, they also have the correct mathematical form to model the thermal decomposition of many polymeric materials (4,5).

Unfortunately, activation energies derived for chemical reactions can be higher or lower than the correct value due to the use of inappropriate kinetic models. While the possible pitfalls are numerous, the one most pertinent to this paper is neglect of the effect of back-reaction, i.e., thermodynamic inhibition, on the apparent activation energy. Vyazovkin mentions this problem in his recent review of solid-state kinetics (6). An example particularly pertinent to this paper is the extremely high activation energies derived using Kissinger's method (7) to measure the kinetics of the β–δ crystallographic phase transition of nitramine octahydro-1,3,5,7-tetranitro-1,3,5,7-tetrazocine (HMX), which occurs at about 175 ^{o}C with an enthalpy of 9.8 kJ/mol.(8) This transition involves a chair-to-boat conformational change, rearrangement of the crystalline lattice from monclinic to hexagonal, and a 6.7% volume increase (9). This problem of deriving the proper activation energy was addressed recently by Henson et al. (10), who report a new kinetic model for the HMX phase transition. An important feature of their model is that the apparent activation energy approaches infinity near the thermodynamic transition temperature as the reaction rate approaches zero.

The objective of the current paper is to evaluate two alternate formalisms for thermodynamically inhibited nucleation-growth reactions. The first is a discrete-particle model, and the second is a phenomenological model in the spirit of Prout and Tompkins (1). We measure kinetics for both individual particles and powdered samples, and we explore the relationships between the two models. Although relationship and utility of the models are demonstrated using the case example of the HMX, we consider the applicability and value of the models to be widespread over both inorganic and organic (including biological) materials.

DESCRIPTION OF KINETIC MODELS

The discrete-particle kinetic model assumes that nucleation occurs at crystal defects and that these defects have a distribution of energies. This defect energy distribution leads to a distribution of nucleation activation energies, which are equal to the activation energy of the defect-free material minus the defect energy distribution, which we describe with a Weibull distribution (Fig. 1). Once nucleated, the growth velocity is governed by an Arrhenius rate constant. The time for an individual crystal to convert is determined by the time at which it initiates and the velocity of the transition wave. The time for an ensemble of crystallites to transform is given by an average over the defect and particle size distributions. Kinetic parameters are derived separately for the nucleation and growth processes of HMX. Although distributed activation energy models, including a Weibull model, are used commonly for fossil fuel chemical kinetics (4), no comparable model appears to exist in the extensive literature for nucleation-growth reactions.

The model was implemented in an Excel spreadsheet using simple explicit numerical integration. The defect energy distribution was represented by 16 discrete reaction channels and used to generate a nucleated fraction versus time. Each of these reaction channels was subdivided into 6 components, which correspond to the initial and final 10% nucleated and four intermediate nucleation probability intervals of 20% each. The growth of each of these nucleated components, in turn, was averaged over 20 evenly spaced growth distances. The model calculations contain some graininess due to the finite number of channels, but not as much as data for mg-sized samples.

While more explicit physically, the detailed model is difficult to calibrate routinely because of the nine reaction parameters needed for ensembles of individual particles. Consequently, we adopted a simpler phenomenological model. The phenomenological model is an extended Prout-Tompkins model having a thermodynamic inhibition term as introduced by Bradley (11) for solid-state reactions and included in the summary paper of Sestak and Berggren on nucleation-growth reactions (12). Our version of this approach is:

$$dx/dt = -kx^{n}(1-qx)^{m}(1-1/K_{eq}) \; . \qquad (1)$$

where x is the fraction remaining, n is a reaction order, m is a nucleation parameter, and q is an initiation parameter. When far from equilibrium and when m=0 and n=1, this reduces to a first-order reaction. The conventional Prout-Tompkins model has n=m=1. The conventional Prout-Tompkins model can be integrated analytically only for constant temperature. The parameter q is related to the initial condition (integration constant) that enables the reaction to get started, since dx/dt is identically zero at x=1 for the Prout-Tompkins model as normally written. Eq. (1) is included in the LLNL kinetics analysis program Kinetics05 (4) and is numerically integrated over the relevant experimental conditions, typically (but not restricted to) isothermal and constant heating, and multiple data sets are fitted simultaneously by nonlinear regression.

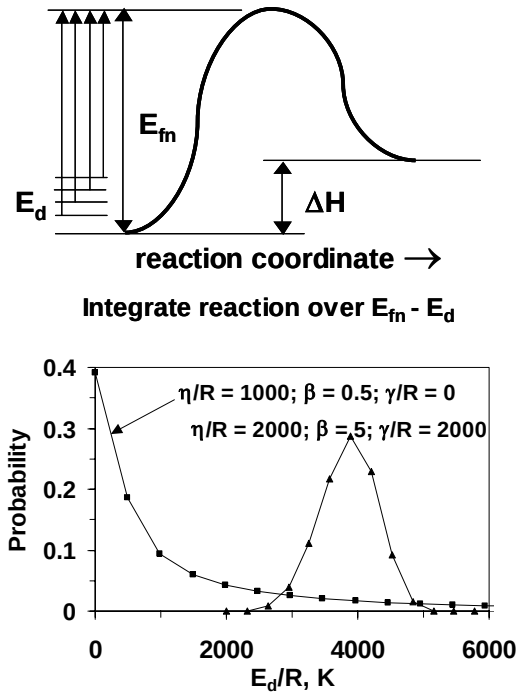

Figure 1. Schematic representation of the defect energy distribution kinetic model, and two examples of defect energy distributions for representative Weibull parameters. β is dimensionless, and η/R and γ/R are in Kelvins.

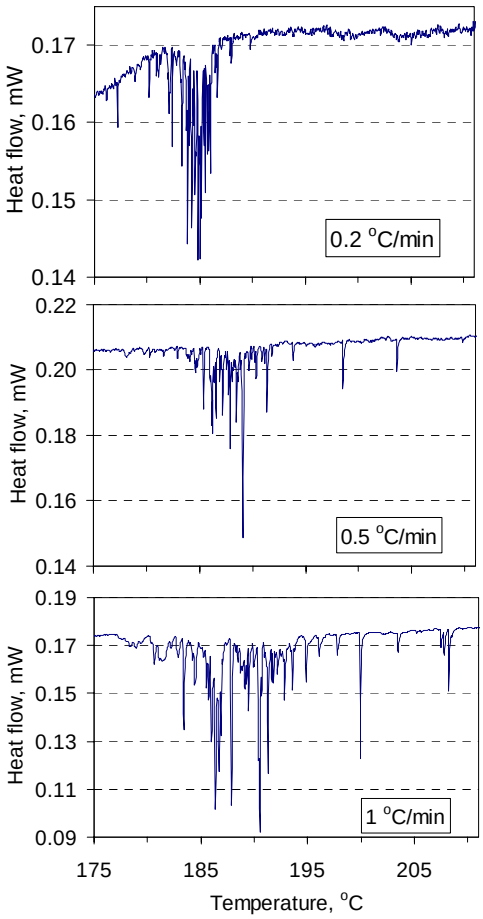

Figure 2. Heat flow thermograms from a differential scanning calorimeter for 0.19 to 0.37 mg samples of HMX batch B-844. The individual spikes are from conversion of individual grains.

EXPERIMENTAL METHODS

Samples

Three sources of pure β-HMX were used in this study. One material (batch B-844) was manufactured by Holston Defense Corporation for Lawrence Livermore National Laboratory using the Bachmann synthesis process and was determined to be >99.90% pure as analyzed by HPLC for RDX impurities. Particle-size analysis indicated that >90% of the material was between 30 and 500 μm in diameter. Other DSC experiments used crystal fragments derived from a large single crystal of β-HMX grown by H. H. Cady and provided to LLNL by the University of Delaware. Fragments averaging 1-mm diameter were used. For the optical studies, pure β-HMX crystals were prepared by the method of Siele et al. (13) Octahydro-1,5-diacetyl-3,7-dinitro-1,3,5,7-tetrazocine (DADN) was treated with 100% HNO_3 and P_2O_5 at 50 °C for 50 min followed by quenching in ice water. Slow recrystallization from acetone yielded HMX as colorless microcrystals.

Reaction Measurements

Optical movies were recorded to help understand earlier AFM experiments (9). A Leica optical microscope (total magnification 800×) was used for the dynamic movies to determine the velocity of the phase transition within individual crystals. The size of each crystal was determined with a calibrated reticle. Movies were recorded in real-time using a color CCD camera and a standard VCR. Sample heating was accomplished using a Veeco temperature controller. The samples were heated from ambient temperature to 300 ^{o}C with a ramp rate of 20 ^{o}C/min. The resolution of the heater stage is 0.2 ^{o}C and the small size of both the sample and the heating stage assures uniform heating over the entire crystal. Movies are available as supplemental material.

A Differential Scanning Calorimeter (DSC), TA Instrument Model 2920, and its associated software, Universal Analysis, were used for additional analyses. All data were collected at 0.2 s^{-1}. DSC (14) measures the difference in the heat flow between a sample and an inert reference as a function of time, where both the sample and reference are subjected to a controlled temperature-pressure environment during that time. The instrument design used here is commonly called the heat flux design. Indium, tin, lead, and zinc from TA Instruments were used to calibrate the temperature and enthalpy response of the instrument at a heating rate of 10 ^{o}C/min. Onset temperatures at other heating rates were corrected using measurements of indium and tin melting points at 0.5, 5, 25 and 100 ^{o}C/min.

All samples were weighed in a Sartorius MC 5 Electronic balance accurate to ≤ 0.005 mg. In all cases, the pan with sample was matched to a reference pan within 100 μg to balance heat flows due to heat capacity.

CALIBRATION OF THE DETAILED MODEL FOR HMX

The nucleation and growth aspects of the detailed model are calibrated separately. We start with general observations followed by a calibration of the growth kinetic parameters, because they are simpler to extract. Nucleation kinetic parameters, which are more difficult to extract, are then estimated.

The reaction rate of the phase transition is assumed to be proportional to heat flow. Representative calorimetry traces are shown in Fig. 2 for 0.4 mg samples of HMX batch B-844. At slow heating rates for small samples, one can discern individual particles undergoing the phase transition. At higher heating rates, the individual grain resolution is lost, because the lower activation energy for growth than for nucleation makes the individual peaks broader in temperature. The distribution of nucleation times reflects the probabilistic nature of nucleation. The envelope outlined by many crystals reflects both the basic rate law (e.g., first-order) for the nucleation process as well as any distribution effects related to particle size, defect energy, or both.

Growth kinetic parameters

Optical movies show that the transformation clearly starts at a specific site then propagates across the crystal. Two shades of textural changes are visible, which was also observed by AFM (9), but they occur close enough in time that the difference does not materially affect the average growth velocity. Approximate contours of the reaction interface as a function of time are given for one crystal in Fig. 3. Although the reaction interface does not propagate smoothly, one can estimate an approximate average reaction velocity for this particle of ~7 μm/s at 178 ^{o}C.

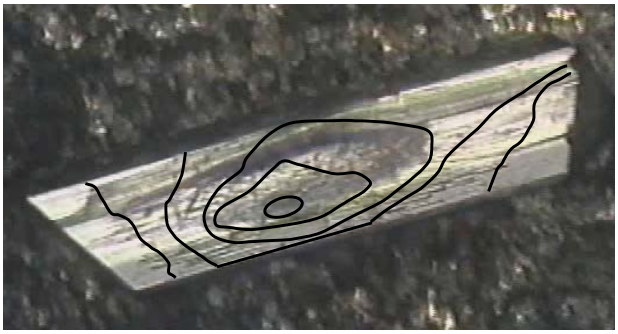

Figure 3. Optical micrograph of 250-μm × 60-μm monoclinic HMX crystal. The phase transition started at about 178 °C. The black contour lines represent an estimate of the reaction interface at 1, 4, 7, 12, and 16 s after nucleation. The total conversion took about 20 s, with a maximum propagation distance of about 140 μm.

To get enough velocity-temperature points to properly determine kinetic parameters, endotherms of individual particles with an average diameter of 1 mm were measured by DSC. Average velocities were estimated from the width of the endotherm (baseline-to-baseline within a few percent) and the particle mass, as measured by simultaneous thermogravimetric and differential thermal analysis. An HMX density of 1.9 g/cm^3 was used. Since the particles are enlongated, the average propagation was assumed to be 1.5 times the effective spherical diameter.

The velocities from both measurement methods are plotted versus 1/T in Fig. 4 for two sources of crystals. The points fit well to the growth analog of Eq. (1), which predicts that the velocity should go to zero at the transition equilibrium temperature.

A corollary prediction of the interfacial velocity going to zero is that the apparent activation energy for growth approaches infinity near the transition temperature. Analyzing the data above and below 192 °C separately yields apparent activation energies of 300 and 60 kJ/mol, respectively, far from and near to the transition temperature. In contrast, taking the thermodynamic inhibition explicitly into account, one derives an uninhibited, forward Arrhenius function for β→δ interfacial growth:

$$k_{fg} = 850 \exp(-3523/T) \text{ mm/s} . \qquad (2)$$

The forward activation energy of 29.3 kJ/mol is three times that of the phase transition enthalpy and 42% of the melting enthalpy. The high-temperature limit of the transition velocity is nearly one m/s, which is substantially lower than the room temperature sound velocity.

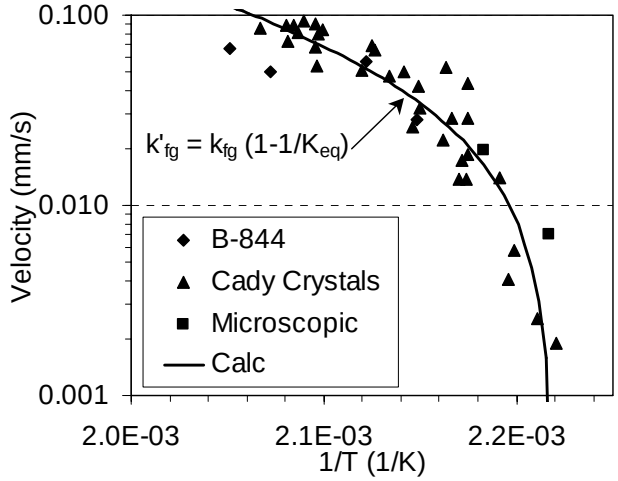

Figure 4. Summary of growth velocity measurements on HMX and a fit to the thermodynamically inhibited growth model, yielding $k_{fg} = 850 \exp(-3523/T)$.

Nucleation kinetic parameters

Given enough individual particle measurements, the curves defined by the cumulative fraction of nucleated particles at different heating rates as in Fig. 2 could be used to directly determine Arrhenius parameters for nucleation. However, powder experiments suffer from reaction-profile overlap and the possibility of cross-particle nucleation. Single particle experiments are too time consuming to gather completely satisfactory statistics. Consequently, the nucleation parameters cannot be determined as accurately as the growth parameters.

Nevertheless, we can explore general limits to the parameters by overlaying the predicted beginning and end of nucleation (1% and 99% points) with the measured onsets for several single particles at each of five heating rates (Fig. 5). After considerable searching, we concluded that only a very high activation energy—greater than 300 kJ/mol—provides a reasonable fit to the data. Such a fit is shown in the bottom of Fig. 5. The data is explained to within the statistical uncertainty of limited nucleation events. No energy defect distribution is apparent at this level of precision. The challenge now becomes to explain the physical interpretation of such a high average energy. As noted previously by Henson et al. (10) this is difficult to understand physically, and they interpret it as a reflection of the ratio of molecules in the active state.

An alternative explanation is that the high activation energy reflects the cooperative motion of several molecules, so the energy per chemical bond is still relatively small. A similar effect is observed for denaturation of proteins, which requires the breaking of many hydrogen bonds along a chain. Effective activation energies sometimes very high (15), giving rise to the concept of an effective cooperative unit. A definitive explanation of the value of the nucleation activation energy is a matter for future exploration.

COMPARISON OF DETAILED AND GLOBAL MODELS FOR HMX

The detailed model can be compared both directly and indirectly to experimental data for HMX. Fig. 6 shows a comparison of the measured fraction converted for batch B-844 versus that calculated by the detailed model. The detailed model was calibrated against certain reaction characteristics of a limited number of Cady crystal fragments (Fig. 5 bottom), not a fit to the reaction profile of a statistically large sample, so the qualitative agreement is confirmation of the validity of the general approach.

Limitations of the data-model concurrence are more pronounced at low heating rates, in part due to the granularity related to the assumption of six nucleation fractions for the interfacial propagation calculations. In addition, low and high temperature tails on the B-844 reaction profiles may reflect the presence of a distribution of defect energies not evident in the calibration against a limited number of nucleation events. As a result, Fig. 7 compares the nucleated fractions directly with the fraction converted, both with and without a small detect energy distribution (η=418 J/mol). To maintain the 50% conversion point at roughly the same temperature, the defect distribution was shifted by its mean (375 J/mol) so that it is roughly symmetrical about zero. An additional factor at the highest heating rates might be thermal gradients within the particles, which would broaden the profile.

Although the detailed model is able to simulate the conversion over wide range of thermal conditions, it is more complicated than desirable for routine application. Consequently, we explored the ability of the thermodynamically inhibited Prout-Tompkins formalism to correlate both synthetic data from the detailed model as well as the experimental data for batch B-844. The results for these two fits are shown in Fig. 8. The global kinetic parameters are

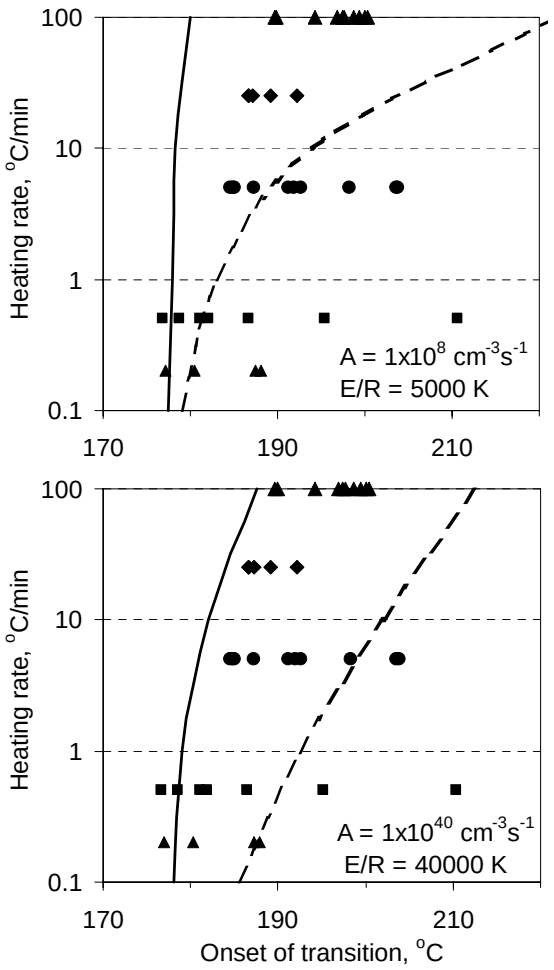

Figure 5. Example of the inability of a first-order nucleation model with low (top) and high (bottom) activation energies to fit the distribution of transition onset temperatures for Cady crystals. A different symbol is used for each heating rate. The solid line represents a 1% nucleation probability and the dashed line represents a 99% nucleation probability, using Eq. 4 and a particle size of 1 mm.

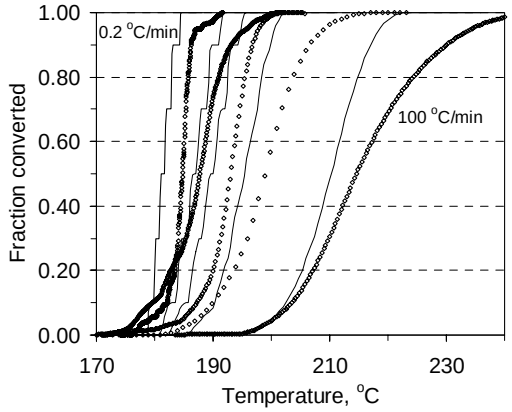

Figure 6. Comparison of the detailed model (lines) calibrated on a small number of Cady crystals to experimental data (points) for HMX batch B-844. The point/line pairs vary from 0.2 °C/min on the left to 100 °C on the right.

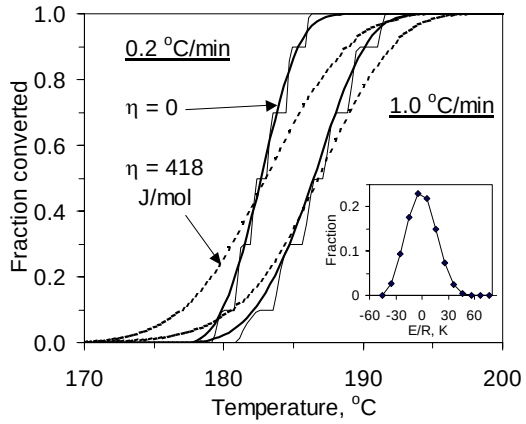

Figure 7. Comparison of the binned nucleation-growth model with detailed nucleated fraction calculations with and without a defect energy distribution, η. β = 3. The effects of a distribution on the early and late conversion is qualitatively similar to that observed for batch B-844 (Fig. 6).

summarized in Table 1. The parameters are very similar for the synthetic and real data. A reaction order of greater than one is mathematically equivalent to a gamma distribution of frequency factors (4), which may reflect a distribution in either particle sizes or defect energies. The apparent activation energy from the nonlinear regression analysis is in between those for nucleation and growth. The higher activation energy from the shift in the 50% conversion temperature is equivalent to using Kissinger's T_{max} method and demonstrates the pitfall of using that method near a thermodynamic transition. The energies from the $T_{50\%}$ method are similar to those reported earlier by Weese et al. (8)

Table 1. Effective kinetic parameters determined from synthetic and real data for the thermodynamically inhibited, extended Prout-Tompkins model.

Data type	Method	A, s^{-1}	E/R, K	Nucleation parameter, m	Reaction order, n
Synthetic Data*	$T_{50\%}$-shift	1.71×10^{44}	49722		
	NLR	1.80×10^{25}	27777	0.299	1.00
HMX B-844	$T_{50\%}$-shift	3.92×10^{37}	42845		
	NLR	2.91×10^{22}	25116	0.180	1.17

*Created using $k_{fn}= 5.23 \times10^{36}\exp(-40000/T)\cdot(1-1/K_{eq})\ s^{-1}$; $k'_{fg}=850\exp(-3523/T)\cdot(1-1/K_{eq})$ mm/s; $K_{eq}=13.8\exp(-2350/T)$.

COMPARISON TO OTHER KINETIC MODELS

Henson et al. (16) derived phase transition kinetics, as measured by second harmonic generation (SHG) during slow heating, for a second-order kinetic model equivalent to a Prout-Tompkins model. They obtained a similar A and E to Brill's group (17). Our activation energy and frequency factor from the modified Prout-Tompkins approach are similar, although slightly higher. However, Henson's first model is not thermodynamically constrained, and we calculate that the phase transition would complete in about 40 min at 160 ^{o}C, which is far below the phase transition.

Both our detailed and global models are similar to the second model of Henson et al. (10) in that a thermodynamic constraint requires the reaction rate to approach zero and the apparent activation energy to approach infinity as the reaction approaches the phase transition temperature. A comparison of calculated half-lives for our two models and their model is shown in Fig. 9. Our global model agrees qualitatively with Henson's model. The 10 ^{o}C difference in transition temperature is probably due to differences between their PBX 9501 formulation and our purer forms.

Saw and Tarver (18) monitored the conversion and reversion of both PBX 9501 and neat HMX by x-ray diffraction (XRD). They observed reversion only in the PBX 9501 and concluded that the reversion is influenced by the polymer binder. Upon repeated cycling, they observed that each successive reversion required a longer time. They also report that complete reversion takes longer than 2 h at 130 ^{o}C, and their data suggest a half-life of about 1 hour. That point is plotted on Fig. 9 and is qualitatively similar to the SHG measurements reported by Smilowitz (19).

Although we did not conduct extensive experiments to characterize the reversion kinetics, we conducted a few experiments in which a crystal was converted, cooled at various conditions, and then heated again to measure the amount reverted. We can estimate a rate constant from the observation that no reversion occurs upon such second heating for times less than 10 hours and that the enthalpy from the 5-day room temperature exposure corresponds to 72% of the ideal value. This implies an approximate value of the half-life of 3 days at room temperature, which is plotted in Fig. 9 and is qualitatively consistent with the model of Henson et al. (10)

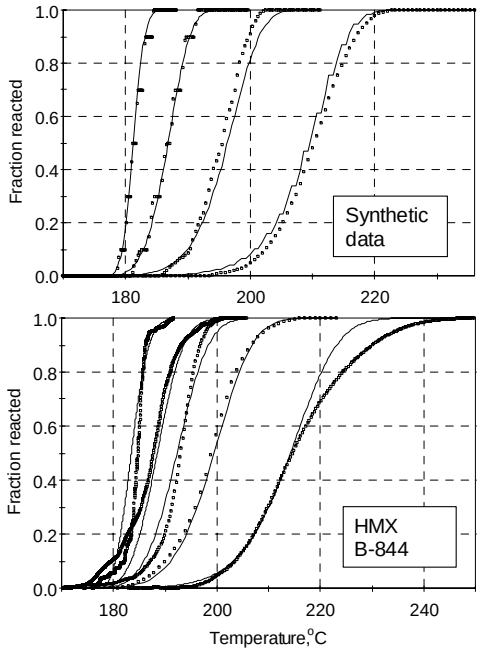

Figure 8. Fit of synthetic from the detailed nucleation-growth model (top) and experimental data for HMX batch B-844 (bottom) to the global thermodynamically inhibited nucleation-growth model. The synthetic data was calculated at 0.1, 1.0, 10, and 100 °C/min, and experimental data is at 0.2, 1.0, 2.5, 10, and 100 °C/min. The resulting kinetic parameters are given in Table 1.

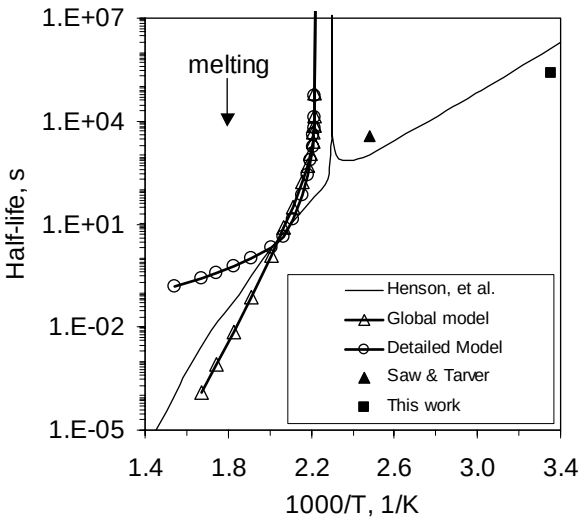

Figure 9. Comparison of the kinetic models of Henson et al. (10) and from this work. All predict that the half-life and activation energy go to infinity close to the transition temperature. The 10 °C difference in transition temperatures can be ascribed largely to the differences in sample. The curvature of the detailed model is due to the assumption of a single nucleation site per grain, which is not universally valid.

SUMMARY

The β→δ crystallographic transition of HMX clearly follows a nucleation-growth mechanism, as can be seen clearly from optical micrographs. Consequently, one can construct a detailed conversion model in which the nucleation and growth processes are treated separately and explicitly. Although the conversion is not reversible along the same reaction pathway to a material with the same physical properties, a thermodynamic inhibition term can be added to both the nucleation and growth kinetic terms that cause the reaction to slow near equilibrium and stop at equilibrium.

When combined, the separately calibrated nucleation and growth kinetics agree with the observed rate of phase transition measured by DSC at heating rates from 0.2 to 100 °C/min. Because of the low activation energy for growth, the profile widths for individual crystals become larger than the spacing between nucleation events, and the reaction profile of an assembly of particles becomes fairly smooth at high heating rates. As particle size increases, the difference between the fraction nucleated and fraction converted becomes substantial for particle sizes on the order of 1 mm at temperatures greater than 200 °C.

While the detailed model is conceptually attractive, it is cumbersome for routine engineering use. Consequently, a phenomenological model has been created by adding the thermodynamic inhibition term to an extended Prout-Tompkins model. This model fits the data well over a wide range of heating conditions, and the apparent activation energy is midway

between those of nucleation and growth. Unfortunately, if one looks at even larger temperature intervals, the phenomenological model is not able to track any change in effective activation energy over the transition from nucleation-dominated kinetics to growth-dominated kinetics.

The concepts of nucleation and growth permeate a wide range of fields. The sigmoidal mathematical form of the Prout-Tompkins model gives it the ability to fit the formation of final product in a sequential reaction (20). It has the ability to fit reaction profiles ranging from linear polymer decomposition to mineral dehydration to the release of implanted gas from solid surfaces (21). Adding a thermodynamic inhibition term should enable it to model the phase transformations in a broad range of organic and inorganic materials over modest temperature intervals near the phase transition.

ACKNOWLEDGMENTS

This work was performed under the auspices of the U.S. DOE by the University of California, Lawrence Livermore National Laboratory under contract number W-7405-Eng-48.

REFERENCES

1. Prout, E. G.; F. C. Tompkins, *Trans. Far. Soc.* **1944**, 40, 488.
2. Avrami, M. J. *J. Chem. Phys*. **1939**, 7, 1103; **1940**, 8, 212; and **1941**, 9, 177.
3. Erofeev, B. V. *C. R. Dokl. Akad. Sci. USSR* **1946**, 52, 511.
4. Burnham, A. K.; Braun, R. L. *Energy & Fuels* **1999**, 13, 1.
5. McCoy, B. J. *Ind. Eng. Chem. Res*. **1999**, 38, 4531.
6. Vyazovkin, S; *Int. Rev. Phys. Chem.* **2000**, 19, 45.
7. Kissinger, H. E. *J. Res. Natl. Bur. Stand.* **1956**, 57, 217.
8. Weese, R. K. Maienschein, J.L., Perrino, C.T. *Thermochim. Acta.* **2003**, 401, 1.
9. Weeks, B. L.; Ruddle, C. M.; Zaug, J. M. and D. J. Cook, *Ultramicroscopy* **2002**, 93, 19.
10. Henson, B. F.; Smilowitz, L.; Asay B. W.; Dickson, P. M. *J. Chem. Phys*. **2003,** 117, 3780.
11. Bradley, R. S. *J. Phys Chem*. **1956**, 60, 1347.
12. Sestak, J; Berggren, G. J. *Thermochim. Acta* **1971**, 3, 1.
13. Siele, V.I.; Warman, M.; Leccacorci, J.; Hutchinson, R.W.; Motto, R.; Gilbert, E.E.; Benzinger, T.M.; Coburn, M.D.; Rohwer, R.K.; Davey, R.K. *Propell. and Explosiv.* **1981** 6, 67.
14. Bershtein, V. A.; Egorov, V. M. *Differential Scanning Calorimetry of Polymers*, Ellis Horwood Limited, **1994**.
15. Miles C. A.; Burjanadze T. V.; Bailey A. J.; *J. Mol. Biol.* **1995**, 245, 248-255.
16. B. F. Henson, B. W. Asay, R. K. Sander, S. F. Son, J. M. Robinson, and P. M. Dickson, *Phys. Rev. Lett.* **1999**, 82, 1213.
17. Karpowicz R. J.; Brill, T. B. *Appl. Spec*. **1983**, 37, 79.
18. Saw C. K.; Tarver C. M.; "Binder/HMX interaction in PBX9501 at elevated temperature," in *Shock Compression of Condensed Matter 2003*, M. D. Furnish, Y. M. Gupta and J. W. Forbes (eds.), AIP Press, **2004**, pp. 1029-1032.
19. Smilowitz, L.; Henson, B. F.; Asay, B. W.; Dickson, P. M., *J. Chem. Phys.* **2003**,117, 3789.
20. Burnham, A. K.; Braun, R. L.; Coburn, T. T.; Sandvik, E. I.; Curry, D. J.; Schmidt, B. J.; Noble, R. A., *Energy & Fuels* **1996**,10, 49.
21. Burnham, A. K. *J. Therm. Anal. Cal.* **2000**, 60, 895.